Revista de Metalurgia 50(3)
July–September 2014, e024
ISSN-L: 0034-8570
doi: http://dx.doi.org/10.3989/revmetalm.024

Effect of natural aging on the microstructural regions, mechanical properties, corrosion resistance and fracture in welded joints on API5L X52 steel pipeline

Benjamín Vargas-Arista[a,✉], Apolinar Albiter[b], Felipe García-Vázquez[c], Óscar Mendoza-Camargo[a], José Manuel Hallen[d]

[a] Instituto Tecnológico de Tlalnepantla, División de Estudios de Postgrado e Investigación, Av. Instituto Tecnológico s/n Col. La Comunidad, Tlalnepantla de Baz, Estado de México, México, C.P. 54070
[b] Instituto Mexicano del Petróleo, Eje Central Lázaro Cárdenas No. 152 Col. San Bartolo Atepehuacan, México D.F. 07730
[c] Corporación Mexicana de Investigación en Materiales, Postgrado en Tecnología de la Soldadura Industrial, Ciencia y Tecnología, 790 Col. Saltillo 400, 25290 Saltillo, Coah. México
[d] Departamento de Ingeniería Metalúrgica, IPN-ESIQIE, Laboratorios Pesados de Metalurgia, UPALM Zacatenco, 07738 México DF, México
[✉] Corresponding author: benjaminvar@yahoo.com.mx

Submitted: 27 September 2013; Accepted: 19 June 2014; Available on line: 03 September 2014

ABSTRACT: A characterization study was done to analyze how microstructural regions affect the mechanical properties, corrosion and fractography of the Heat Affected Zone (HAZ), weld bead and base metal for pipe naturally aged for 21 years at 30 °C. Results showed that microstructures exhibited damage and consequently decrease in properties, resulting in over-aged due to service. SEM analysis showed that base metal presented coarse ferrite grain. Tensile test indicated that microstructures showed discontinuous yield. Higher tensile strength was obtained for weld bead, which exhibited a lower impact energy in comparison to that of HAZ and base metal associated with brittle fracture by trans-granular cleavage. The degradation of properties was associated with the coarsening of nano-carbides observed through TEM images analysis, which was confirmed by SEM fractography of tensile and impact fracture surfaces. The weld bead reached the largest void density and highest susceptibility to corrosion in H_2S media when compared to those of the HAZ and base metal.

KEYWORDS: API5L X52 steel; Coarsening; Degradation; HAZ; Natural aging

Citation / Cómo citar este artículo: Vargas-Arista, B., Albiter, A., García-Vázquez, F., Mendoza-Camargo, O., Hallen, J.M. (2014) "Effect of natural aging on the microstructural regions, mechanical properties, corrosion resistance and fracture in welded joints on API5L X52 steel pipeline". *Rev. Metal.* 50(3): e024. doi: http://dx.doi.org/10.3989/revmetalm.024.

RESUMEN: *Efecto del envejecimiento natural sobre la microestructura, propiedades mecánicas, resistencia a corrosión y fractura en uniones soldadas de acero para tubería API5L X52*. Se realizó un estudio de caracterización para analizar cómo la microestructura afecta a las propiedades mecánicas, corrosión y fractura de la zona afectada por calor (ZAC), soldadura y metal base para tubería envejecida naturalmente durante 21 años a 30 °C. Los resultados indicaron que las microestructuras presentaron daño y consecuentemente reducción en propiedades mecánicas, como consecuencia del envejecimiento por servicio. El estudio mediante MEB mostró que el metal base presenta grano ferrítico grueso. La prueba de tensión indicó que las microestructuras mostraron fluencia discontinua. La mayor resistencia a la tracción se presentó en la soldadura, la cual alcanzó menor energía de impacto en comparación con la ZAC y metal base asociado con fractura frágil por clivaje transgranular.

La degradación de las propriedades está en relación con el engrosamiento de nanocarburos observados a través del análisis de imágenes por MET, lo que se confirmó mediante fractografía por MEB de superfícies de fractura bajo tensión e impacto. La soldadura alcanzó la mayor densidad de microhuecos y la mayor susceptibilidad a la corrosión en un medio conteniendo H_2S que cuando se compara con la ZAC y metal base.

PALABRAS CLAVE: Acero API5L X52; Degradación; Engrosamiento; Envejecimiento natural; ZAC

1. INTRODUCTION

API 5L steel pipeline is extensively used for gas, hydrocarbons and crude oil transportation in the petroleum industry, which are generally designed for a service life of about 20 years. This type of pipeline is manufactured using microalloyed steel with Nb, Ti and V. The Thermo-Mechanically Controlled rolling Process (TMCP) is commonly employed to control strain induced precipitation, dislocation networks and strengthening through the precipitation of niobium carbonitrides (Vargas *et al*., 2011). This kind of pipeline is fabricated with a longitudinal welding which is performed using a double pass submerged arc welding process. As with most alloys, this steel is also subjected to a natural aging phenomenon during periods of time at room temperature, which is likely to be accelerated by the service conditions within the range of 25 to 70 °C, producing changes in the microstructure and mechanical properties after long-term service (Vargas *et al*., 2007). The aging process is described by a peak-aged condition associated with strengthening precipitation from particles; and afterward an over-aging state that is related to the decrease in strength and the coarsening of precipitates after extended periods of time (Vargas *et al*., 2009).

There are also reports on carbon steels indicating that artificial aging induced by isothermal treatment can be performed at 100 to 350 °C to accelerate the natural aging (Krauss, 1990). Homma *et al*. (1998) reported that low strength steel is susceptible to aging at 250 °C for 1 hour which is equivalent to 2 years of natural aging. There is some research on aging of ferrous alloys like API 5L steel pipe line that has aimed to give an understanding of the causes and effects of aging, such as the deterioration or degradation of the micro-structural features, research which was correlated and evaluated by non-destructive methods such as ultrasonic testing (Vargas *et al*., 2012). Some studies are related to the weld metal of multipass steel aged at 550 °C for 30,000 hours, in which the fine grain microstructure in the Heat Affected Zone (*HAZ*), shows structural changes such as the agglomeration and coarsening of precipitates (Watanabe *et al*., 2004). A second case is the 17 GS steel pipeline with a diameter of 720 mm that transported oil, and which after 30 years of service displayed significant decrease in the Charpy absorbed energy, approximately 40% at room temperature (Kotrechko *et al*., 2004). A third case is the coarsening study of nano-sized $M_{23}C_6$ carbide precipitate in 2.25Cr–1Mo steel found in boiler tube specimens subjected to extended aging of up to 160,000 hours at 540 °C in a thermal power plant. It is found that the coarsening of these nano-particles reflected in a diffraction pattern as crystallite size increased with aging resulted in material degradation (Jayan *et al*., 2004). Additionally, a study on the artificial aging of API 5L X52 welded steel carried out at 250 °C for up to 1,000 hour resulted in an increase of the general corrosion rate in a solution of brine containing hydrogen sulphide at 25 °C for the weld bead, HAZ and the base metal as the aging time elapsed. The higher corrosion rate was linked to the coarsening of trans-granular nano-particles of cementite and niobium carbide for weld bead and base metal respectively for long aging times (Vargas *et al*., 2011).

The objective of this study is to characterize the changes in the microstructure, mechanical properties and corrosion resistance in the weldment regions of the weld bead, HAZ and base metal of the aforementioned steel, as a result of the aging in-service conditions. The contribution of this research is to provide further experimental information that will be useful in understanding the micro-structural and mechanical degradation of commercial aged pipeline taking into account the chemical composition of the fluid transported.

2. EXPERIMENTAL PROCEDURE

Longitudinal welded joint specimens were obtained from API5L X52 steel pipeline naturally aged which was 27.9 mm in thick and 609.6 mm in nominal diameter and which transported heavy oil at an operating pressure of 60 Kg cm^{-2}. The pipe was welded longitudinally using a semi-automatic Submerged Arc Welding process (SAW) with a double-pass through and X-groove configuration using a steel electrode and flux under API 5L (2008) Welding Procedure Specification (WPS).

The chemical composition, determined by atomic absorption spectrometry and direct combustion method, of the weld bead in the natural aged condition was inside the range of criteria for acceptance by AWS A5.17 (2004). The base metal fell outside the criteria of 1.40% Mn maximum and

0.32% C_{eq} maximum according to API 5L (2008) therefore the mechanical resistance and weldability were affected, see Table 1.

For micro-structural characterization, the specimens were machined, ground, polished and subsequently etched using a Nital at 2% solution to reveal the micro-structural features using a JEOL 6300 Scanning Electron Microscope (SEM). The morphological, structural and chemical characterizations were achieved using a JEOL-2000FX-II Transmission Electron Microscope (TEM), which was equipped with energy dispersion spectroscopy, operated at 200 kV. Therefore, thin foils of 3 mm diameter were prepared by grinding and jet polishing until perforated, using a twin-jet electro-polisher model 110 with a 30% HNO_3 + 70% CH_3OH solution kept at −55 °C during the operation.

Specimens of the weld bead, HAZ and base metal were cut and machined according to the mechanical test type. For evaluation of the Vickers hardness in three different microstructures, transversal specimens having 27.9 mm in width and 50 mm in length were used. This testing was performed with a FM-7 future Tech Corp. micro-hardness tester applying a 2.9 N load and repeating every reading 20 times, as per ASTM Standard E384 (2005). For the weld bead, Vickers hardness was tested in the both passes of the welding cycle.

The round longitudinal specimens for uniaxial tensile testing had a 6 mm gage diameter and a 50.8 mm gage length. Each specimen was completely machined from the weld bead, HAZ and base metal. This testing was carried out on a 100 kN, AG-10TG Shimadzu machine under displacement control at an average strain rate of approximately 1.6×10^{-4} s^{-1} and the displacement was measured by a SG 50–50 extensometer at room temperature, in accordance with ASTM Standard E8M (2008). For the weld bead, the tensile property measurements were made in the first and root passes of the welding cycle. In the case of the HAZ the measurements included all the sizes and different heterogeneous microstructures, resulting in mean tensile properties. Three tensile specimens were taken for each region of the welded joint aged.

In order to characterized the impact absorbed energy, specimens were machined with reduced type-A Charpy toughness, rectangular cross section, transverse orientation, a calibrated thickness of 7.5 mm, a width of 10 mm, a length of 55 mm and a V-notch at 45° located along the central line of the weld bead, HAZ and base metal. The toughness tests were carried out on a C Otto Wolpert-Werke PW 30/15K-type pendulum impact machine at −10 °C and in triplicate for each micro-structural region, as per ASTM Standard E-23 (2006).

The tensile and impact fractured specimens of the base metal, HAZ and weld bead were analyzed using a JEOL 6300 SEM in order to reveal the relevant micro-features causing fracture type in the specimens. The microscope was operated at 20 kV, 220 μA, using a secondary electron and working distance of 39 mm.

For the corrosion evaluation, square transversal electrodes with surface area of 1 cm^2 were taken from the three micro-structural zones and mounted in epoxy resin to ensure the area of exposure. Electrodes were prepared using the metallographic technique and were degreased with ethanol before immersion in the corrosion medium. The aqueous solution of H_2S synthetic brine was prepared according to NACE ID-182 (1995). This brine allows simulating an environment containing hydrogen sulfide with concentration of 500 mg L^{-1}. The Tafel polarization electrochemical technique was performed with the glass cell formed by three-electrodes including working electrodes machined from the weld bead, HAZ and base metal, a Saturated Calomel Electrode (SCE) of fixed potential of 0.2415 V and a graphite bar as auxiliary electrode. The potentiodynamic polarization measurements were made using an EG&G Applied Research model 273 A potentiostat controlled by a computer with PAR M352/252 corrosion analysis software. This testing was carried out by polarizing the electrode approximately at ± 250 mV from the Open Circuit Potential (OCP) using a slow scan rate of 0.166 mV s^{-1} at 25 °C. All the above tests were performed in static condition. The general corrosion rate (V_{corr}) was calculated from i_{corr} by using equation (1), according to ASTM standard G-102 (2004).

$$V_{corr} = 0.0033\ (i_{corr}\ EW/d) \quad (1)$$

where V_{corr} is the corrosion rate (mm y^{-1}); i_{corr} the corrosion current density (μA cm^{-2}); EW the equivalent weight of the corrosion species (g) and d the density of the corrosion species (g cm^{-3}).

TABLE 1. Chemical composition (wt. %) of the weld bead and base metal

	Element (Wt. %)								
Material	**C**	**Mn**	**Si**	**Nb**	**Ti**	**V**	**P**	**S**	**C_{eq} †**
Weld bead	0.070	1.34	0.40	0.050	0.020	0.010	0.023	0.021	0.295
Base metal	0.086	1.48	0.25	0.005	0.020	0.010	0.029	0.010	0.333

†$C_{eq} = C + \frac{Si}{30} + \frac{Mn}{20} + \frac{Cu}{20} + \frac{Ni}{60} + \frac{Cr}{20} + \frac{Mo}{15} + \frac{V}{10}$

3. RESULTS AND DISCUSSION

The welded joint of naturally aged API 5L X52 pipeline exhibited a deterioration in its properties as the Charpy impact energy with the formation of brittle fractures in cleavage zones on the surfaces impacted, micro-structural damage appearing as coarsening of nano-particles and carbide plates, and growth of ferrite grain size. Therefore, this pipeline showed relevant micro-structural deterioration and mechanical degradation.

3.1. SEM micro-structural analysis

SEM images of the longitudinal joint welded by the Submerged Arc Welding (SAW) process on API 5L X-52 steel pipe as shown in Figure 1. The SEM observations show that the weldment region, produced by double submerged arc welding, was formed by three different microstructures as shown in Figure 1a. The weld bead (Fig. 1b) exhibited a solidification of the microstructure resulting from the welding cycle, which was composed of large columnar ferrite grains oriented in the direction of the heat flow (dark areas), acicular ferrite (white areas) between columnar grains (Hamada and Yamauchi, 2002) and an important percentage of non-metallic inclusions having an average diameter of 1.5 μm within the columnar grains (white points).

The HAZ of the second zone generated by the double welding thermal cycle (Fig. 1c) showed a heterogeneous recrystallized microstructure located near the fusion line, formed mainly by fine acicular ferrite (white areas) and coarse-grained ferrite (dark areas). The complete HAZ showed an average width of 4 mm (Homma *et al*., 1998). The as-hot rolled microstructure of the base metal showed the rolling direction and it was formed by an equiaxed ferritic matrix (dark areas) with coarse grain size and pearlite colonies (white areas) with a percentage of each constituent of about 70 and 30, respectively (Fig. 1d). The average measurement of ASTM grain size number G was determined to be about 8.55 in accordance with ASTM Standard E-112 (2004). Therefore, the base metal showed over-aging, which was associated with the large ferritic grain size as a consequence of grain growth.

3.2. TEM micro-structural analysis

Figure 2 shows typical TEM bright field images of the HAZ and base metal structure, respectively. Figure 2a exhibits the presence of medium-sized nearly cuboidal Ti particles, (see corresponding EDS spectrum in Figure 2b), from 20 to 40 nm in size that were located within the ferrite grains of the HAZ structure of the secondary recrystallized zone produced by the welding thermal cycle during welding.

For the base metal we observed that there were medium-sized nearly circular shaped Nb-C particles from 10 to 25 nm in size within ferrite grains, as indicated in the TEM image and its corresponding EDS spectrum in Figures 2c and 2d, respectively. These

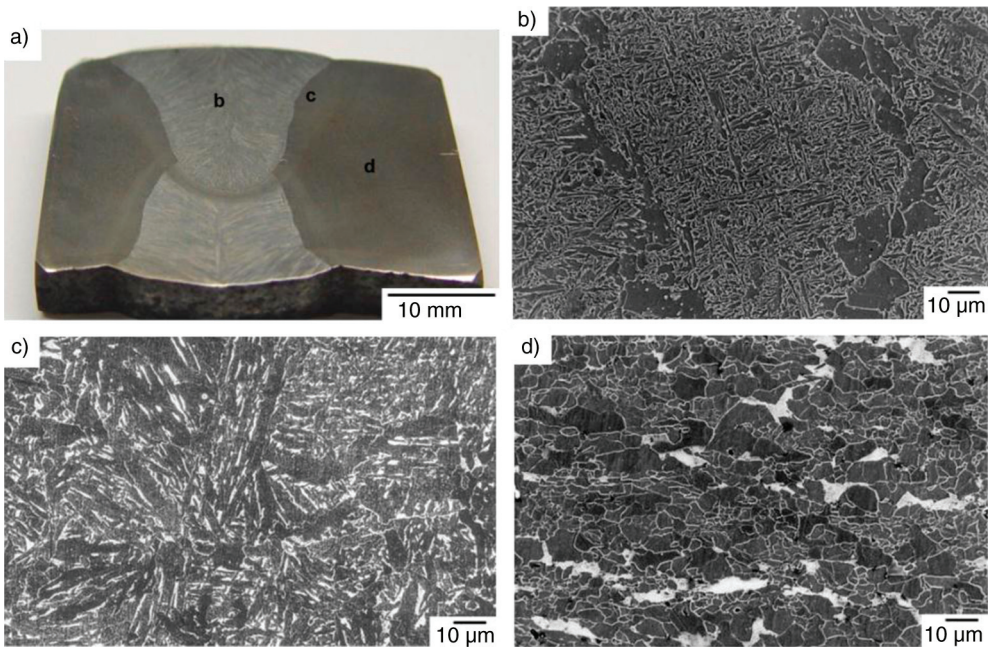

FIGURE 1. SEM micrographs: (a) an SAW welded joint naturally aged, (b) large columnar grains in the weld bead solidified, (c) fine acicular ferrite in the HAZ of second zone recrystallized and (d) ferritic matrix in base metal showing a transversal section of rolling direction.

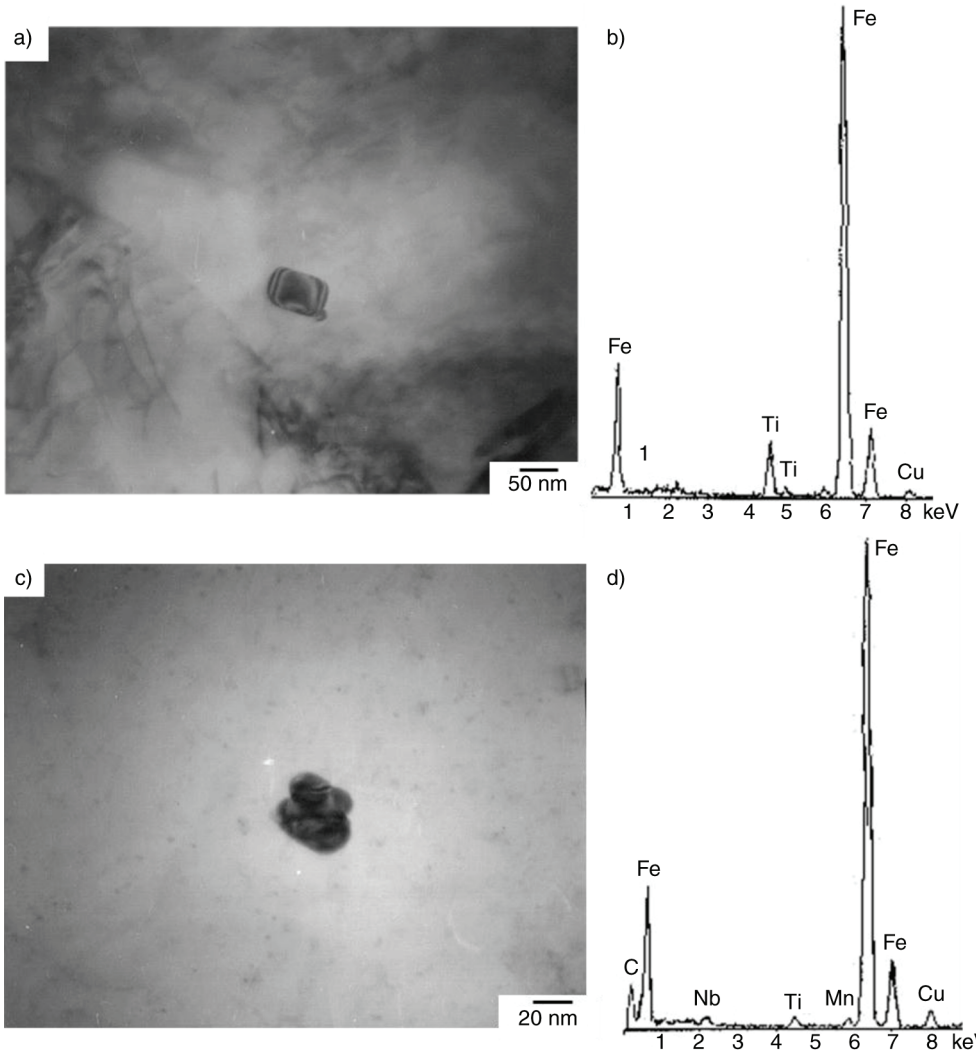

FIGURE 2. TEM bright field (BF) images obtained from welded joint naturally aged: (a) cuboidal Ti nano-particle, (b) its corresponding EDS spectrum showing Ti peaks in the HAZ, (c) nearly rounded Nb-C rich particle and (d) its EDS spectrum indicating Nb and C peaks for the base metal.

nano-particles could be from the strain induced precipitation and their size could be associated with the natural aging effect.

Moreover, TEM observations revealed the presence of large, coarse and inter-granular Fe-C plates (dark lines) located in ferrite grain boundaries of the micro-structural zones of weld bead, base metal and HAZ under study, as can be seen in the images of Figure 3 and its corresponding EDS spectrum with the characteristics peaks of Fe and C in Figure 3d, which was related with the growth process favored by the service conditions. The structural different was the amount and thickness of these plates within the structures analyzed. This clearly shows that the base metal had the largest amount of Fe-C plates compared to the HAZ and weld bead.

Additionally, TEM image analysis was performed on the micro-structural zones, which revealed the presence of large, nearly rounded, trans-granular nano-particles, as reported in Saucedo *et al*. (2003), which exhibited preferential nucleation sites among dislocations within the ferrite grains. A typical TEM image of the weld bead showed large particles with sizes ranging from 10 to 35 nm in dislocations (Fig. 4a). The EDS spectrum displayed the characteristic Fe and C peaks (Fig. 4b), which corresponded to the particle marked in Figure 4a. The structural characterization of these Fe-C nano-particles revealed that these were cementite-type compound reported elsewhere (Vargas *et al*., 2006).

The density and size of the nano-carbides, and volume fraction of inter-granular carbide plates were measured. The number of particles per μm^2 was calculated by counting the particles and their size was directly measured. The fraction of plates was determined by the volumetric difference between

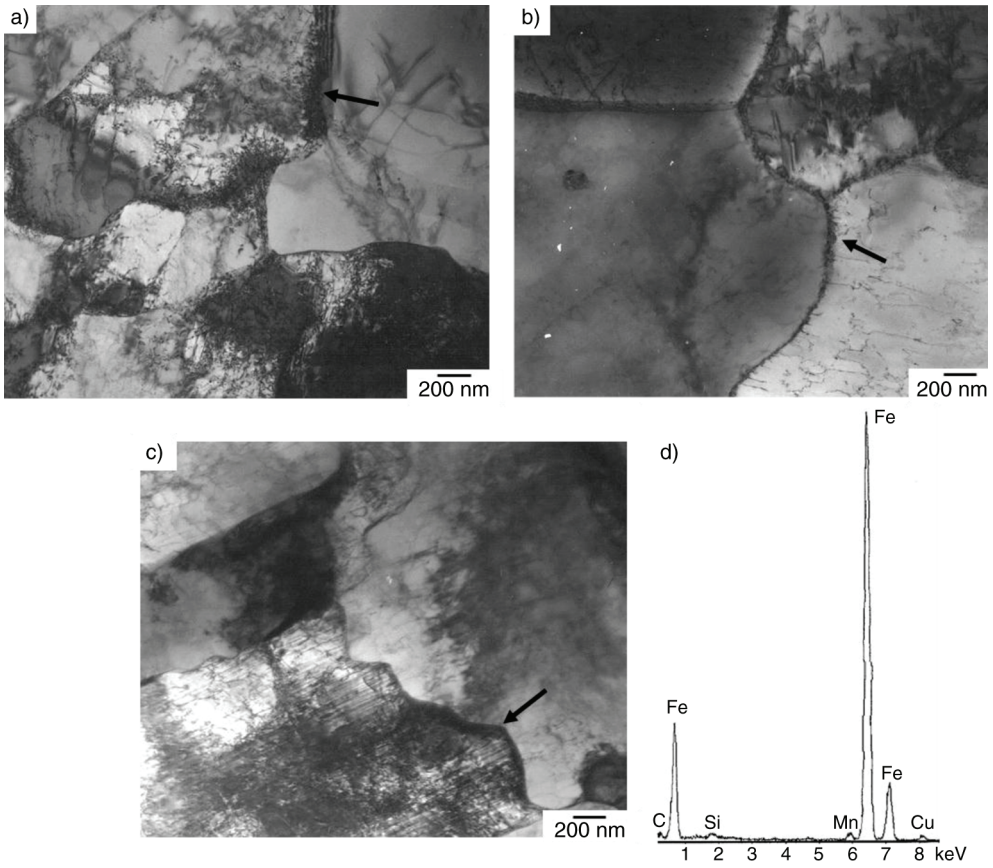

FIGURE 3. TEM bright field images of inter-granular iron carbide plates obtained from the welded joint naturally over-aged: (a) weld bead, (b) base metal, (c) HAZ and (d) its EDS spectrum indicating Fe and C peaks, with different amount and thickness within the ferritic grain boundaries.

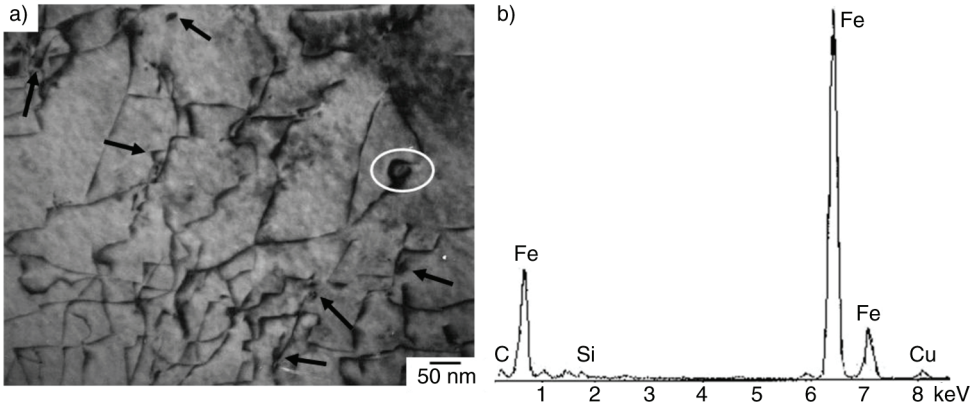

FIGURE 4. TEM bright field image obtained from the weld bead naturally over-aged: (a) coarsening of nano-particles between dislocations and (b) EDS spectrum indicating Fe and C peaks.

the plates and matrix. The values of these measurements are listed in Table 2. The analysis showed that the base metal had the largest carbide density, followed by weld bead and HAZ due to the particles generated by the TMCP rolling process contributing to this density (Vargas *et al*., 2006). The weld bead and HAZ showed similar carbide size which was larger than that of the base metal related to the SAW welding cycle and thermal effect of the natural aging. Finally, the base metal reached the highest volume fraction of carbide plates compared to that of the HAZ and weld bead, which was associated

TABLE 2. Carbide density, mean particle size and inter-granular carbide for the weld bead, HAZ and base metal

Material	Nano-carbide density (particles μm^{-2})	Mean carbide size (nm)	Inter-granular carbide fraction volume (%)
Weld bead	17.67	22.5	1.85
HAZ	15.95	22.5	2.33
Base metal	27.16	15	2.38

with the strain induced strengthening during the TMCP process.

According to the values listed in Table 2 and aforementioned TEM image analysis, the HAZ and base metal exhibited nano-sized particles and carbide plates with notable coarsening (Jayan *et al*., 2004, Watanabe *et al*., 2004) i.e., an increase in their size related to the over-aged condition (Vargas *et al*., 2006) as a consequence of long periods of time as 21 years. The coarsening process of particles was described by the Ostwald ripening process spoken by Moon *et al*. (2006). A growth of the larger nano-particles at the expense of the other smaller ones was observed. The new large particles had weak interactions between dislocations, resulting in a more plastic deformation and a decrease in the yield strength.

3.3. Characterization of the mechanical properties

The stress-strain curves of the weld bead, HAZ and base metal showed a discontinuous yielding behavior with well-defined upper and lower yield strengths, as can be seen in Figure 5. The weld bead presented a higher ultimate tensile strength and larger discontinuous yielding than that of the HAZ and base metal, which was associated with the aging phenomenon.

The mechanical analysis showed that the yield and tensile strengths, elongation, Vickers hardness and Charpy energy of three micro-structural zones were modified with the natural aging at 30 °C after 21 years of service. The values of these properties, versus the criteria for acceptance of the specifications, are listed in Table 3. The weld bead reached the highest mechanical properties, such as the micro-hardness, yield and tensile strengths compared to the HAZ and base metal. However, it exhibited inferior impact energy as elongation values than the HAZ and base metal, as a consequence of the prolonged thermal effect of aging. Therefore, the weld bead didn't reach the minimum energy requirement of 27 J and the elongation showed the minimum value of the AWS A5.17 (2004). The base metal exhibited an elongation to fracture lower than that of the minimum value of API 5L (2008).

According to literature related to natural aging process and the properties values given in Table 3, the HAZ and base metal showed micro-hardness values corresponding to deterioration of the Vickers hardness. The weld bead reached a yield strength, as well as the base metal and weld bead exhibited

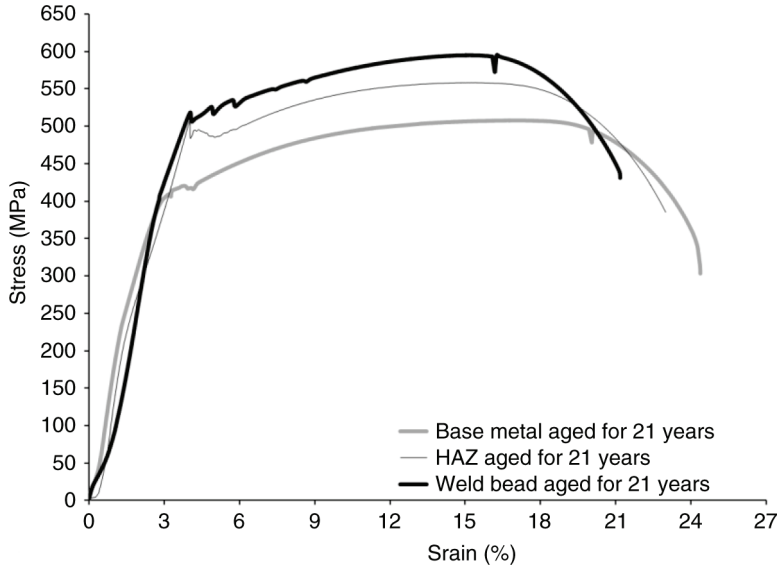

FIGURE 5. Stress vs. strain curves for the weld bead, HAZ and base metal under over-aged condition at 30 °C after 21 years of service.

TABLE 3. Mechanical properties of the weld bead, HAZ and base metal

Material	Vickers hardness HVN (HRC)	σ_o 0.2% σ_{max} (MPa)	Elongation (MPa)	Charpy Energy %	Charpy Energy at −10 °C (J)
Weld bead	231 (18.4)	524	606	22	12
HAZ	219 (15.3)	466	557	24	121
Base metal	192 (9.1)	403	503	25	130

lower elongation values attributed to the existence of over-aging. Finally, the absorbed energy for the three micro-structural regions showed lower values. This mechanical behavior suggests a degradation of Vickers hardness, elongation and impact energy (Kotrechko *et al.*, 2004, Vargas *et al.*, 2008). All these were linked to the coarsening process of nano-carbides and carbide plates under natural over-aged condition.

3.4. Fractography analysis

Additional indirect measurements of the micro-structural changes involving the density and size of nano-particles were achieved through SEM observations of fracture surfaces obtained from the tensile fractured specimens for the weld bead, HAZ and base metal. The fracture surfaces exhibited a ductile-type failure with well-defined micro-void morphology, which was linked to the mechanism of nucleation, growth and coalescence of micro-cavities (Vargas *et al.*, 2009), as can be observed in Figure 6. The micro-cavity nucleation centers were promoted by the presence of carbides and non-metallic inclusions.

To evaluate the fracture mechanism on the specimens, the average density and diameter of voids were measured. The number of voids per μm^2 was calculated by counting the micro-voids and their diameter was directly measured. Therefore, ten fields of view were counted for these fracture parameters. The measurements are listed in Table 4. The fractured surfaces of the weld bead showed higher void density and lower diameter compared to that in the HAZ and base metal, due to the inferior growth of micro-voids, deteriorated impact energy and higher yield strength.

Considering the natural aging process, we can see that weld bead and HAZ reached void density values corresponding to an over-aged state. While the weld bead and base metal showed void diameter measurements related to over-aging. Both fracture parameters were associated with the coarsening of nano-carbides after long periods of time, such as 21 years.

The reduction in impact energy after natural aging was confirmed using SEM fractographic analysis of the impact fractured surfaces of the

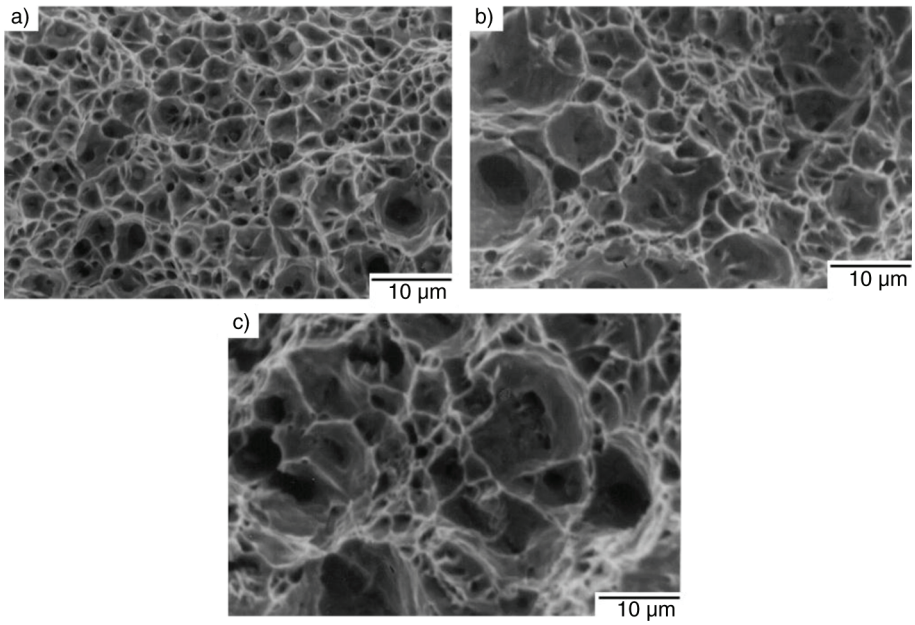

FIGURE 6. Fractography of tensile fractured specimens for the welded joint naturally over-aged state: (a) weld bead, (b) HAZ and (c) base metal, with different density and diameter of micro-void within surface.

TABLE 4. Density and diameter of micro-voids for the weld bead, HAZ and base metal

Material	Micro-void density (voids μm^{-2})	Micro-void diameter (μm)
Weld bead	0.134	4.43
HAZ	0.097	5.02
Base metal	0.065	5.27

weld bead, HAZ and base metal. The middle surfaces showed mixed fracture composed principally of brittle fracture due to trans-granular cleavage with well-defined facets and ductile fracture with morphology of networks including small intergranular micro-voids located at the boundaries of facets, as can be observed in Figure 7 for the weld bead, HAZ and base metal. The brittle fracture through cleavage was produced as a consequence of the natural aging conditions, which showed a significant difference in the amount for the three micro-structural zones. The weld bead exhibited a larger amount of cleavage within the fracture surfaces (Fig. 7a), followed by the HAZ (Fig. 7b) and base metal (Fig. 7c).

3.5. Corrosion behavior

Corrosion resistance of the welded joint was investigated using Tafel polarization in a solution of brine containing hydrogen sulfide at 25 °C. The corrosion rate (V_{corr}) values, according to equation (1), for three micro-structural zones, are listed in Table 5. The weld bead showed a high slightly generalized corrosion rate (Vargas *et al*., 2011) followed by the HAZ and base metal, i.e., if the base metal is the reference, the percentage of variation from HAZ and weld bead is 4.7% and 9.5%, respectively.

The SEM study of the corrosion products at the three different micro-structural regions confirmed the corrosion behavior explained. We observed the presence of brittle and porous oxide and iron sulphur on the metallic surface. The corrosion showed in the weld bead can be attributed to the presence of shallow corrosion products with higher brittleness and porosity, as indicated in the SEM micrograph and its corresponding EDS spectrum in Figure 8. The base metal reached a corrosion rate corresponding to a condition of over-aged, which was linked to the coarsening process of nano-carbides and porous corroding products favoring the electrochemical corrosion process.

4. CONCLUSIONS

The weld bead, heat affected zone and base metal were susceptible to natural aging during 21 years of service at 30 °C, affecting their microstructure, mechanical properties, corrosion resistance and fracture behavior, as a results of the damage from the over-aged state.

The micro-structural regions showed a dominant process called coarsening of trans-granular

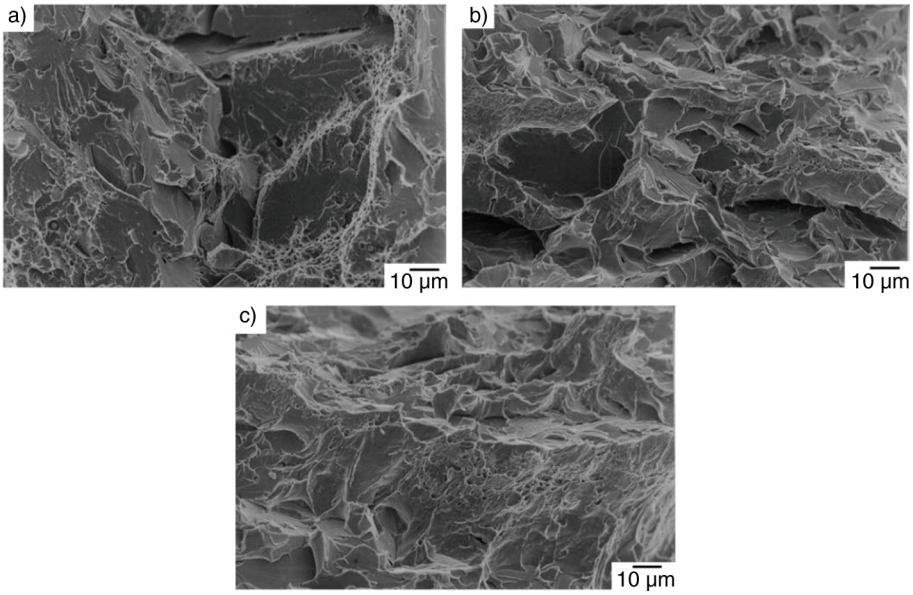

FIGURE 7. Fractography of impact fractured specimens for the welded joint naturally over-aged: (a) weld bead, (b) HAZ and (c) base metal, with different amount of cleavage brittle fracture.

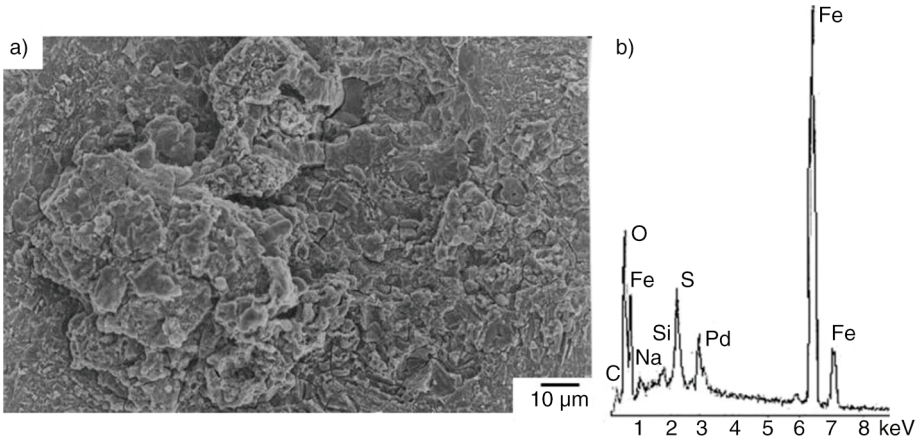

FIGURE 8. SEM micrograph obtained from the weld bead naturally over-aged: (a) corrosion products with larger brittle and porous on the corrosion specimen and (b) its corresponding EDS spectrum showing Fe, S and O peaks.

TABLE 5. Corrosion rate in H_2S media at 25 °C for the weld bead, HAZ and base metal

Material	Corrosion rate V_{corr} (mm y^{-1})
Weld bead	0.254
HAZ	0.243
Base metal	0.232

medium nano-particles and inter-granular carbide plates, i.e., an increase in the particle and plate size, which was unfavorable to the mechanical properties and fracture mechanism. The base metal showed a notable coarse ferritic grain size while the weld bead showed larger carbide size as a consequence of the over-aging exposition after several years.

The elongation was deteriorated for the base metal and weld bead, which reached a drastic reduction in the absorbed energy compared to that of the applied specifications. These properties degradation was related to the presence of brittle fracture zone associated with the trans-granular cleavage in the impact fractured surfaces, with major amount of cleavage for the weld bead, followed by the HAZ and base metal. Thus, the natural aging favored the brittle fracture under impact load.

The particle coarsening observed in the welded joint, which acted as nucleation sites of micro-cavities, was confirmed through the fracture parameters of density and size of micro-voids in the tensile fractured specimens with higher void diameter and lower void density as a result of the over-aged state. The base metal reached minor void density and major void diameter followed by the HAZ and weld bead, which were linked to the larger nano-carbide density that favored the higher amount of cavities to form larger voids.

The resistance to corrosion of the damaged three micro-structural zones decreased resulting in the slight increase in the general corrosion rate due to larger brittle and porous corrosion products of iron oxide and sulfide for the weld bead compared to the HAZ and base metal.

ACKNOWLEDGEMENTS

The authors wish to thank the experimental and financial supports received from the IPN and CONACyT.

REFERENCES

API 5L (2008). *Specification for Line Pipe*, 44th Ed., American Petroleum Institute, Washington D.C., USA, pp. 8–17.

ASTM Standard G-102 (2004). *Standard Practice for Calculation of Corrosion Rates and Related Information from Electrochemical Measurements*. ASTM International, West Conshohocken, PA, USA, pp. 1–5. http://dx.doi.org/10.1520/G0102-89R04E01.

ASTM Standard E-112 (2004). *Standard Test Methods for Determining Average Grain Size*. ASTM, West Conshohocken, PA, USA, pp. 10–12.

ASTM Standard E-384 (2005). *Standard Test Method for Microindentacion Hardness of Materials*. ASTM, West Conshohocken, PA, USA, pp. 1–8.

ASTM Standard E-23 (2006). *Standard Test Methods for Notched Bar Impact Testing of Metallic Materials*. ASTM, West Conshohocken, PA, USA, pp. 2–8.

ASTM Standard E-8M (2008). *Standard Test Methods for Tension Testing of Metallic Materials*. ASTM, West Conshohocken, PA, USA, pp. 7–18.

AWS A5.17 (2004). *Specification for Carbon Steel Electrodes and Fluxes for Submerged Arc Welding*. American Welding Society, Miami FL, USA, pp. 2–4.

Hamada, I., Yamauchi, K. (2002). Sensitization behavior of type 308 stainless steel weld metals after postweld heat treatment and low temperature aging and its relation to microstructure. *Metall. Mater. Trans. A* 33 (6), 1743–1754. http://dx.doi.org/10.1007/s11661-002-0183-5.

Homma K., Miki C., Yang, H. (1998). Fracture toughness of cold worked and simulated heat affected structural steel. *Eng. Fract. Mech*. 59 (1), 17–28. http://dx.doi.org/10.1016/S0013-7944(97)00100-8.

Jayan, V., Khan, Y.M., Husain, M. (2004). Coarsening of nano sized carbide particles in 2.25Cr–1Mo power plant steel after extended service. *Mater. Lett*. 58 (21), 2569–2573. http://dx.doi.org/10.1016/j.matlet.2004.02.051.

Kotrechko, O.S., Krasowsky, Y.A., Meshkov, Y.Y., Torop, M.V. (2004). Effect of long-term service on the tensile properties and capability of pipeline steel 17GS to resist cleavage fracture. *Int. J. Pres. Ves. Pip*. 81 (4), 337–344. http://dx.doi.org/10.1016/j.ijpvp.2004.02.015.

Krauss, G. (1990). *Heat treatment and processing principles*. ASM Materials, Park OH, USA, pp. 125–130.

Moon, J., Lee, Ch., Uhm, S., Lee, J. (2006). Coarsening kinetics of TiN particle in a low alloyed steel in weld HAZ: considering critical particle size. *Acta Mater*. 54 (4), 1053–1061. http://dx.doi.org/10.1016/j.actamat.2005.10.037.

NACE ID-182 (1995). *Wheel Test Method Used for Evaluation of Film-Persistent Corrosion Inhibitors for Oilfield Applications*. NACE, 1440 South Creek Drive, Houston, USA, pp. 1–4.

Saucedo, M.L.M., Komazaki, I.S., Hashida, T., Shoji, T., Lopez, H.V.M. (2003). Aplicación del ensayo miniatura de embutido para la evaluación de la tenacidad a temperaturas criogénicas de aceros inoxidables austeníticos envejecidos isotérmicamente. *Rev. Metal*. 39 (5), 378–386.

Vargas, A.B., Albiter, A., Angeles, Ch.C., Hallen, J.M. (2006). Effect of the artificial aging time on the mechanical properties of weldment on API 5L X-52 line pipe steel. *Metall. Mater. Trans. A*. 37 (9), 2683–2690. http://dx.doi.org/10.1007/BF02586102.

Vargas, A.B., Hallen, J. M., Albiter, A. (2007). Effect of the artificial aging on the microstructure of weldment on API 5L X-52 steel pipe. *Mater. Charact*. 58 (8–9), 721–729. http://dx.doi.org/10.1016/j.matchar.2006.11.004.

Vargas, A.B., Hallen, J.M., Albiter, A., Angeles, Ch.C. (2008). Degradation of impact fracture during accelerated aging of weld metal on microalloyed steel. *Rev. Metal*. 44, 485–492. http://dx.doi.org/10.3989/revmetalm.0747.

Vargas, A.B., Angeles, Ch.C., Albiter, A., Hallen, J.M. (2009). Metallurgical investigation of the aging process on tensile fracture welded joints in pipeline steel. *Mater. Charact*. 60 (12), 1561–1568. http://dx.doi.org/10.1016/j.matchar.2009.09.007.

Vargas, A.B., Solis, R.J., Angeles, Ch.C., Albiter, A., Hallen, J.M. (2011). Deterioration of the corrosion resistance of welded joints in API5L X52 steel isothermally aged. *Int. J. Electrochem. Sci*. 6 (2), 367–378.

Vargas, A.B., Balvantin, A., Baltazar, A., García, V.F. (2012). On the use of ultrasonic spectral analysis for the characterization of artificially degraded API 5L X52 steel pipeline welded joints. *Mat. Sci. Eng. A*. 550, 227–234. http://dx.doi.org/10.1016/j.msea.2012.04.064.

Watanabe, T., Yamazaki, M., Hongo, H., Tabuchi, M., Tanabe, T. (2004). Effect of stress on microstructural change due to aging at 823 K in multi-layer welded joint of 2.25Cr-1Mo steel. *Int. J. Pres. Ves. Pip*. 81 (3), 279–284. http://dx.doi.org/10.1016/j.ijpvp.2003.12.017.